Soft Matter

# Betweenness Centrality as Predictor for Forces in Granular Packings



| | |
|---|---|
| Journal: | *Soft Matter* |
| Manuscript ID | SM-ART-07-2018-001372.R2 |
| Article Type: | Paper |
| Date Submitted by the Author: | 20-Dec-2018 |
| Complete List of Authors: | Kollmer, Jonathan; North Carolina State University, Department of Physics<br>Daniels, Karen; North Carolina State University, Department of Physics |
| | |

Soft Matter

ARTICLE TYPE

Cite this: DOI: 10.1039/xxxxxxxxxx

# Betweenness Centrality as Predictor for Forces in Granular Packings †

Jonathan E. Kollmer,*[a] and Karen E. Daniels[a]

Received Date
Accepted Date

DOI: 10.1039/xxxxxxxxxx

www.rsc.org/journalname

A load applied to a jammed frictional granular system will be localized into a network of force chains making inter-particle connections throughout the system. Because such systems are typically under-constrained, the observed force network is not unique to a given particle configuration, but instead varies upon repeated formation. In this paper, we examine the ensemble of force chain configurations created under repeated assembly in order to develop tools to statistically forecast the observed force network. In experiments on a gently suspended 2D layer of photoelastic particles, we subject the assembly to hundreds of repeated cyclic compressions. As expected, we observe the non-unique nature of the force network, which differs for each compression cycle, by measuring all vector inter-particle contact forces using our open source PeGS software. We find that total pressure on each particle in the system correlates to its betweenness centrality value extracted from the geometric contact network. Thus, the mesoscale network structure is a key control on individual particle pressures.

## 1 Introduction

For idealized granular particles in a jammed configuration, there are many different ways for the force and torque balance on each particle to be satisfied for any given packing geometry and boundary conditions: this is known as the force network ensemble.[1,2] A key reason for this ensemble of configurations is that particles deform at their contacts, and thereby store information about their loading history;[3,4] the rate- and asperity-dependence of real frictional contacts make this an even more prevalent effect.[5]

Generally speaking, the inter-particle forces within these materials are mathematically under-determined: particle positions are insufficient to determine the force network. Furthermore, while two packings might have the same occupied volume or internal pressure, they can nonetheless have vastly different bulk material properties.[6–8]. Therefore, a promising approach is to make predictions for the physical properties of granular materials using tools and concepts from statistical physics,[9] by directly considering the ensemble of states. However, the choice of the correct ensemble remains the subject of active research.[4,10–14]

Importantly, the transmission of forces occurs primarily via linear structures running through a series of connected particles (see Fig. 1), forming a *force network*. This network provides the granular material with structures at many scales, from the particle (micro) scale to the force chain (meso) scale to the bulk (macro) scale. The mesoscale force network contains only a subset of the particles, and yet carries most of the load. Because these force chains can span significant portions of the system, it becomes inadequate to use either local or mean field approaches to describe the systems behavior.[16,17] Thus, it is attractive to focus attention on force networks[18–21] within jammed granular packings.

In order to make quantitative predictions about the role of force networks, it is useful to draw on the field of network science[22–25] in addition to statistical mechanics or grain-scale solid mechanics. Mathematical networks are often represented as a graph consisting of nodes and edges.[22] In the case of a granular system, each node would represent a particle, and edges connect two particles (nodes) which share a contact. In many cases, it is informative to weight each edge by its contact forces; here we consider binary (unweighted) networks. These techniques have recently been applied in a variety of granular contexts ranging from shear to compression to vibration[25–31] and a summary of the many applications can be found in a recent review.[32]

As shown in Fig. 1, the force chain network that results from repeated experiments on the same particle network is both variable in the details, and repeatable in other aspects. For instance, the same two particles on the right side are often in strong contact with the wall. Thus, while the force-configuration fluctuates around several preferred states, some particles are loaded more often than others and the configurations are not completely ran-

[a] *Department of Physics, North Carolina State University, Raleigh, NC, USA. E-mail: jekollme@ncsu.edu*

† Electronic Supplementary Information (ESI) available: [details of any supplementary information available should be included here]. See DOI: 10.1039/cXsm00000x/

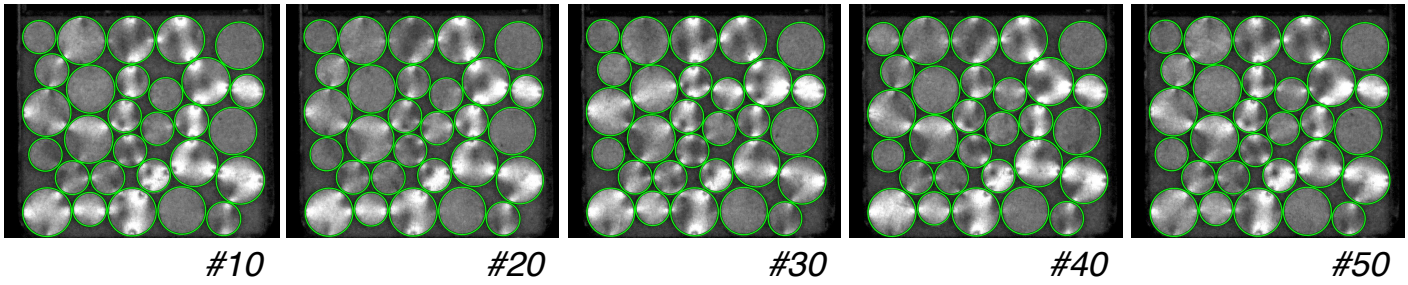


**Fig. 1** Five representative loading cycles for the same configuration of a granular packing, with $N = 29$ photoelastic disks floated on an air table. In these darkfield images taken in polarized light, brighter particles are those with higher contact forces.[15] Particle outlines are superimposed as green circles.

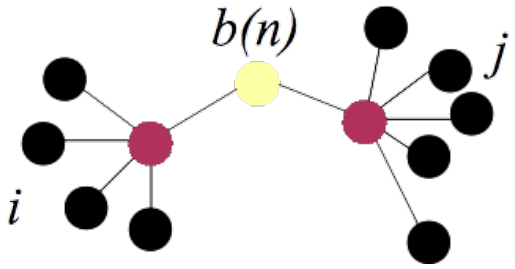


**Fig. 2** Schematic illustration of the concept of betweenness centrality, with each node color-coded by its $b$ value (brighter corresponds to larger values). The bright node at the center has high a high value of $b$ because many shortest-paths between any other two particles have to go through it. The dark nodes (here, arranged at the edges for clarity) have $b = 0$, since they never act as connecting nodes.

dom. This raises the question of what properties of the particle packing make it more or less likely for a particular particle to bear a strong load.

This variability suggests that prior studies of the statistics of inter-particle contact forces[3,33,34] arise through simultaneously sampling two ensembles: the positions of the particles, and the valid configurations of forces. While there have been a few experiments probing granular ensembles,[4,35] it has been difficult to decouple the external load that probes the force network from other forces acting upon the system, like gravity or basal friction.[36] The experiments described here examine the distribution of forces in a loaded granular system, isolated from the effects of configuration.

In order to understand how the variability in force networks arises, we focus on a mesoscale, nonlocal, measure of the network connectivity: the betweenness centrality $b$.[37] As shown schematically in Fig. 2, the betweenness centrality of particle (node) $n$ is calculated by considering the extent to which shortest-paths between two other nodes must travel through that node. Mathematically, this is defined as the fraction of shortest path $s_{ij}$ along the edges (contact forces) between any two nodes $i \neq n \neq j$ in the system that goes through node (particle) $n$:

$$b(n) = \sum_{i \neq n \neq j} \frac{s_{ij}(n)}{s_{ij}}. \quad (1)$$

In the results presented here, we performed our calculations using the open-source functions provided by the Brain Connectivity Toolbox.[38] In all plots, we plot the values of $b$ normalized to the largest $b$ across all cycles within that dataset, to better allow for comparison between datasets with different particle configurations. Note that $b$ depends only the adjacency network of the particles, rather than the inter-particle forces. This quantity, therefore, allows us to test how particle-scale forces depend on mesoscale connectedness. We find that $b$ can be used to predict the typical force on a particle, averaged over an ensemble of realizations.

## 2 Experiment

Our experiment is designed to generate and characterize many different force configurations within a quasi-two-dimensional, hyperstatic (under-constrained) granular packing at constant volume. To minimize extraneous external forces, we utilize a horizontal layer of photoelastic disks floating on a gentle air cushion.[39] This creates an effectively gravity-free system without basal friction. The particles are laterally confined inside a piston that can apply an uniaxial load to the packing, via a series of quasi-static steps of constant wall-displacement.

A schematic drawing of the experimental setup is provided in Fig. 3. Each experimental run consists of cyclically loading and unloading the packing by a small enough wall displacement that (1) there is no change the nearest-neighbor particle configuration, but (2) the force network is erased between cycles. From cycle to cycle, there are microscopic changes in the contact points on the particles, but there are no neighbor changes. The initial volume $V_0$ was chosen to be just before the onset of jamming (zero pressure), and the final volume so that the mean contact force rises to approximately 0.5 N. This maximum compression (minimum volume) was chosen to provide a balance between two effects: large enough forces to show a fully-developed network with good force resolution, but small enough forces to suppress internal rearrangements and out-of-plane buckling. For the experiments presented here, we uniaxially compress the packing in steps of constant volume ($\Delta x = 0.2$ mm, corresponding to $\Delta V = 0.002869 V_0$). Each step is a quasistatic step in order to allow us to disregard inertial effects.

The granular material is composed of a bidisperse mixture of two different radii particles ($r_1 = 5.5$ mm and $r_2 = 7.6$ mm) to suppress crystallization. Between runs, the particle positions are

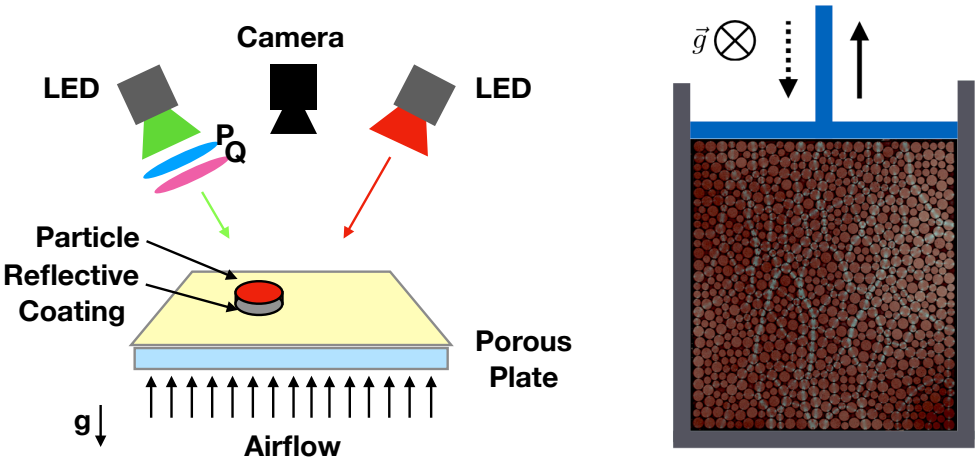


**Fig. 3** Experimental apparatus. Left: Photoelastic particles are floated on a horizontal air table to suppress the influence of gravity and basal friction, and visualized from above. Illumination in the red channel is unpolarized, providing imaging of the particle positions. Illumination in the green channel is polarized, providing visual access to the internal stress field within each particle. The red and green color channels of the camera can later be separated to process particle positions and force information from a single color image. Right: The grains are placed within a horizontal piston, and cyclically compressed. Particle positions are visible in red, and force chains in cyan.

randomized. We conduct experimental runs to generate an ensemble of force networks on two complementary system sizes: $N = 29$ or $N = 824$ particles. The $N = 29$ particle system allows for hundreds of repetitions and high resolution imaging (which in turn allows for very precise force reconstruction), while the $N = 824$ particle system allows for sampling an ensemble further away from the boundaries of the system. The drawback of the larger system size, however, is that it is hard to re-compress the packing while also maintaining the same particle configuration;[40] we find that only about one hundred cycles are typically possible.

After starting an experiment, we discard the data for the initial $\approx 100$ cycles to get rid of the most prominent aging effects. After this initial annealing period, the force continues to fluctuate around a well-defined mean while the particle configuration remains unchanged. For each compression cycle we take one image of the system, at a resolution of $2299 \times 2506$ pixels.

In order to measure the vector contact forces on each particle, we utilize particles made of a photoelastic material (Vishay PhotoStress PSM-4, elastic modulus $E = 4$ MPa). Photoelastic materials have the property of rotating the polarization of transmitted light, by a known amount that depends on the local stress tensor. Therefore, it is possible to fit a theoretical model to images of the modulated light intensity within individual particles, and thereby obtain the vector contact force at each contact.[3,15,35] We perform this step using our open source tool PeGS (Photoelastic Grain Solver) which is freely available on GitHub.[41] As a result, we get two vectorial contact forces for each contact in the system ($\vec{F}_{ab}$ and $\vec{F}_{ba}$) since each side of a contact is processed individually. We then run PeGS again, giving the average of both forces as an initial guess. As a final result we then compare the residual of the force fit from both runs and pick the result with the smaller residual. This is to improve fitting accuracy and remove outliers. In order to measure the total pressure on each particle we calculate

$$P = \mathrm{Tr}(\hat{\sigma}) \qquad (2)$$

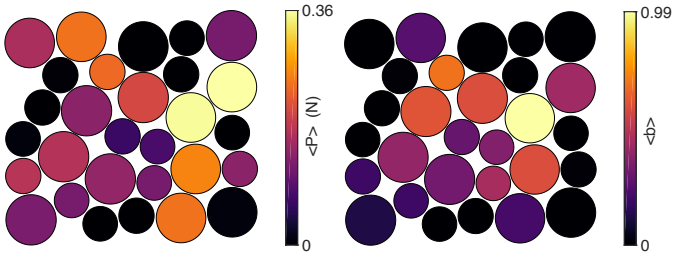


**Fig. 4** Graphical representation of the average pressure $\langle P \rangle$ (left) and the betweenness centrality $\langle b \rangle$ (right) on each particle in an $N = 29$ system. Averages are taken over 900 realizations of the configuration. Betweenness centrality values have been normalized to the largest $b$ across all cycles of the dataset (see text).

where $\hat{\sigma}$ is the stress tensor, derived from the photoelastic analysis.

In order to calculate network measures, we operate on the binary contact (adjacency) matrix for each image. This is formed by identifying all contacts in the system for which we detect a nonzero value for the absolute force between two particles. We carefully checked that changing this threshold to 0.01 N or 0.001 N does not significantly change the results presented in this paper. At the end of the paper, we will additionally explore the successful use of a particle-separation criteria as an alternative method.

## 3 Results

Figure 4 shows an analysis a typical run from the $N = 29$ particle system illustrating the main result. In the left panel, each particle is colored by its mean pressure $\langle P \rangle$, averaged over the ensemble of 900 images in the run. Bright particles are those that are reliably on a strong force chain. In the right panel, each particle is colored by its average betweenness centrality value $\langle b \rangle$, obtained from the contact network. We take the average although the binary contact network barely fluctuates (i.e. the experiment was designed to avoid neighbor changes so most of the fluctuation

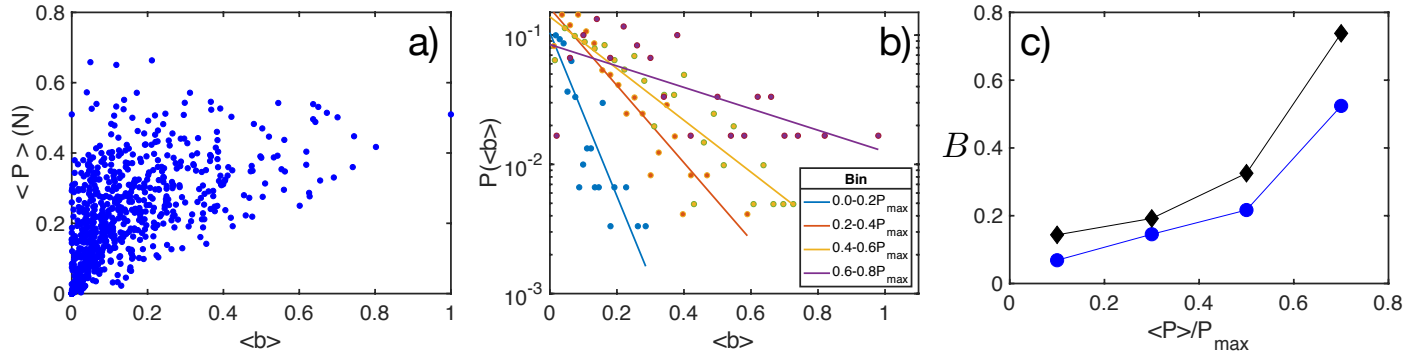


**Fig. 5** (a) Mean pressure $\langle P\rangle$ as a function of betweenness centrality $\langle b\rangle$, for each particle in an $N = 824$ system. Betweenness centrality values have been normalized to the largest $b$ across all cycles of the dataset (see text). (b) Histogram of betweenness centrality values within four different pressure bins (symbols) from a), together with fits to Eq. 3 (lines). Each color represents a different bin. (c) Characteristic betweenness centrality value $B$, obtained from the fits shown in panel (b) (blue circles) and a second dataset (black diamonds) using the same system but a different particle configuration. Pressures were averaged over 88 (blue) and 48 (black) realizations of the same particle configuration.

is in magnitude of force). Visually, we observe the presence of correlations between the bright particles in both images.

Next, we quantitatively explore this correlation using data from the $N = 824$ particle system. Fig. 5a shows a scatter plot of $\langle b\rangle$ vs. $\langle P\rangle$ for each particle in the system, with averages taken across 88 realizations (cycles) of the force network for a single particle-configuration. We quantify this positive correlation by finding a Pearson correlation coefficient $c_R = 0.60$ ($p = 1.3\times10^{-81}$). We repeat the experiment with a different configuration for 48 cycles and again get strong correlation results of $c_R = 0.47$ ($p = 6.1\times10^{-46}$). For the $N = 29$ particle system the correlation yields $c_R = 0.75$ ($p = 2.3\times10^{-6}$). All three examined systems show a statistically-significant correlation.

To better visualize the underlying trend, we sort all data from a single experiment into four bins corresponding to four different pressure ranges. Fig. 5b shows a histogram of the corresponding measurements of betweenness centrality $\langle b\rangle$, taken within each of these four bins. We observe that each of these four bins has a histogram following an exponential decay of the form

$$P \propto e^{-\langle b\rangle/B} \tag{3}$$

where $B$ is the characteristic value for that pressure range. As shown in Fig. 5c, this relationship is a monotonically increasing function, with the largest pressures (strongest, most reliable force chains) being particularly associated with large values of $\langle b\rangle$. Fig. 5c contains data from both datasets of the $N = 824$ particle system. Data from the $N = 29$ particle dataset (providing 29 values of $\langle b\rangle$) is too small to be suitable for this statistical evaluation.

The relationship between $\langle b\rangle$ and $\langle P\rangle$ establishes an underlying connection between the system's microscale (particle-scale pressure) and mesoscale (contact network) via the betweenness centrality parameter. This correlation makes physical sense by considering two very basic assumptions: that particles transmit force along inter-particle contacts, and that particles which have more such paths going through them will be more likely to accumulate forces from other particles. This relationship is only probabilistic,

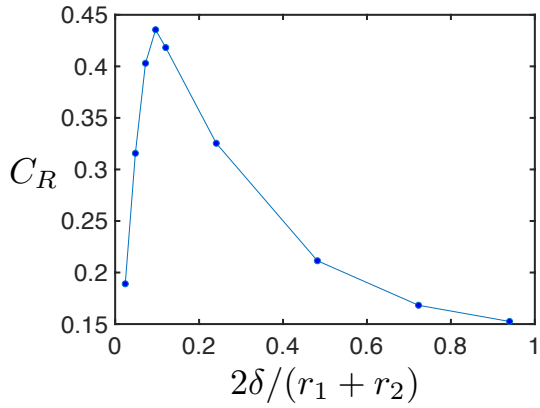


**Fig. 6** Pearson correlation coefficient $c_R$ between the mean pressure $\langle P\rangle$ and the betweenness centrality $\langle b\rangle$, for each particle in the $N = 824$ system, as a function of the particle separation threshold $\delta$. This is the same dataset as used in Fig. 5a, but for this analysis $\langle b\rangle$ is calculated from the geometric contact network rather than from thresholded forces.

however, since any given configuration of particles is (1) compatible with an ensemble of force networks[1,2] and (2) contains forces which are history-dependent.[3,42–45] This, while there is a clear positive correlation, there is also significant scatter in the data.

Finally, we perform a stronger test of whether using thresholded force data to determine the contact network predetermined this successful result. Using purely geometric data (rather than the photoelasticity of the particles), we measure the separation $\delta = |\vec{x}_i - \vec{x}_j| - (r_i + r_j)$ between all pairs of adjacent $i, j$ particles. We then apply a threshold to $\delta$ to determine whether two particles are specified as being in contact. This gives an adjacency matrix that varies as a function of $\delta$, and now caries the meaning of neighbor network rather than a strict contact network. We create a set of these adjacency matrices with different values of $\delta$, and for each one calculate $\langle b\rangle$ using Eq. 1. We then repeat the analysis shown in Fig. 5a for each value of $\delta$. As shown in Fig. 6, our analysis remains valid for any $2\delta \approx 0.1(r_1 + r_2)$. This resolution is consistent with the resolution of the Hough trans-

form used to identify the particle positions (approximately 1/10 of a particle radius). From this analysis of neighbor networks, we observe that it is only necessary to identify particles that are close enough to be likely touching, rather than experimentally confirming each contact. Because definitive determination of contacts is challenging for many experiments on foams, colloids, and grains, the successful use of betweenness centrality without access to inter-particle forces opens the possibility to perform future studies on non-photoelastic particles.

## 4 Discussion and Conclusions

We have designed an experiment that shows how a network measure known as betweenness centrality can predict the forces on a particle. Our predictions are tested using ensembles averaged over many realizations of the force network for a given particle configuration. The betweenness centrality provides a new way to relate mesoscopic network features[27,46] to microscopic particle configurations. Therefore, its statistical moments might provide a simple tool for predicting such granular properties as the contact force distribution $P(f)$, heat transport coefficients,[47] and the speed of sound.[48,49]

We have also showed that we can extract the necessary contact network information to make these predictions from purely geometric information, without the need for detailed photoelastic or other contact-force measurements. Whether or not force-network prediction can be done from only knowing particle positions has been a recent issue of debate.[50–52] Here, we illustrate how to use experimentally-measured (imperfect) adjacency information to make probabilistic predictions for the inter-particle forces. We observe that this can be done without knowing the exact radii of each particle,[51] unlike the analytical solution of Gendelman *et al.*[50] which is intractable under realistic circumstances. This insensitivity to contact measurements can be seen in Fig. 6, where even with 20% error in radii measurements there is a strong correlation present.

Importantly, we also observe variations in the force network among the different samples in the ensemble (see (Fig. 1). Therefore, only statistical predictions make sense. However, the remaining variability is likely related to such phenomena as Branley's coherer, in which there is observed to be significant sensitivity of the electrical and thermal conductivity of metallic granular materials in response to electromagnetic waves.[53]

In this paper, we have isolated a single problem that can be addressed by network science techniques: the determination of how the inhomogeneous force response of a granular material under uniaxial loading can be inferred from its contact or neighbor network. We hope that centrality-based approaches will also be useful for other particulate and amorphous systems where the material explores an ensemble of configurations. For instance, where dramatic or localized changes occur as a result of force chain rearrangements in fragile[54], polydirectionally stable[55] or sheared systems[7,8,56,57]. Furthermore, because centrality measures are able to identify the nodes/edges through which large forces will more likely pass, they may also prove useful in forecasting locations at which localized failures will occur under loading, for instance through cage-breaking[58]. A key advantage would be that these measures require much less information than dynamical soft spots[59] or Coulomb failure[60], making them experimentally-tractable. Finally, it would be important to understand which of these features are reproducible in numerical simulations, for which frictional contacts are not necessarily the same as in experimental systems.

## Conflicts of Interest

There are no conflicts of interest to declare.

## Acknowledgements

We gratefully acknowledge James Puckett for the design and construction of the air table on which the apparatus is based, and for the inspiration for the new parallelized version of the contact-force code. We further acknowledge Estelle Berthier for helpful discussions. This research was supported by the James S. McDonnell Foundation and the NSF through grants DMR-0644743 and DMR-1206808.

## References

1 J. H. Snoeijer, T. J. H. Vlugt, M. van Hecke and W. van Saarloos, *Phys. Rev. Lett.*, 2002, **92**, 54302.
2 B. P. Tighe, J. H. Snoeijer, T. J. H. Vlugt and M. van Hecke, *Soft Matter*, 2010, **6**, 2908.
3 T. S. Majmudar and R. P. Behringer, *Nature*, 2005, **435**, 1079.
4 E. S. Bililign, J. E. Kollmer and K. E. Daniels, *Phys. Rev. Lett. (in press)*, 2018.
5 S. Dillavou and S. M. Rubinstein, *Phys. Rev. Lett.*, 2018, **120**, 224101.
6 S. Dagois-Bohy, B. P. Tighe, J. Simon, S. Henkes and M. van Hecke, *Phys. Rev. Lett.*, 2012, **109**, 095703.
7 R. Pastore, M. P. Ciamarra and A. Coniglio, *Philosophical Magazine*, 2011, **91**, 2006–2013.
8 R. Pastore, M. P. Ciamarra and A. Coniglio, *Granular Matter*, 2012, **14**, 253–258.
9 D. Bi, S. Henkes, K. E. Daniels and B. Chakraborty, *Annual Review of Condensed Matter Physics*, 2015, **6**, 63.
10 R. Blumenfeld and S. F. Edwards, *Journal of Physical Chemistry B*, 2009, **113**, 3981–3987.
11 B. P. Tighe, A. R. T. van Eerd and T. J. H. Vlugt, *Physical Review Letters*, 2008, **100**, 238001.
12 B. P. Tighe and T. J. H. Vlugt, *Journal of Statistical Mechanics: Theory and Experiment*, 2011, **4**, 04002.
13 Y. Wu and S. Teitel, *Physical Review E*, 2015, **92**, 022207.
14 S. Sarkar, D. Bi, J. Zhang, J. Ren, R. P. Behringer and B. Chakraborty, *Physical Review E*, 2016, **93**, 042901.
15 K. E. Daniels, J. E. Kollmer and J. G. Puckett, *Rev. Sci. Inst.*, 2017, **88**, 051808.
16 M. E. Cates, J. P. Wittmer, J.-P. Bouchaud and P. Claudin, *Chaos*, 1999, **9**, 511–522.
17 K. Ramola and B. Chakraborty, *J. Stat. Phys.*, 2017, **169**, 1–17.
18 S. N. Coppersmith, C.-H. Liu, S. Majumdar, O. Narayan and T. A. Witten, *Phys. Rev. E*, 1996, **53**, 4673–4685.
19 J. E. S. Socolar, D. G. Schaeffer and P. Claudin, *Eur. Phys. J. E*,

2002, **7**, 353–370.
20 J. F. Peters, M. Muthuswamy, J. Wibowo and A. Tordesillas, *Phys. Rev. E*, 2005, **72**, 041307.
21 E. T. Owens and K. E. Daniels, *Europhys. Letters*, 2011, **94**, 5.
22 M. E. J. Newman, *Networks: An Introduction*, Oxford University Press, Oxford, UK, 2010.
23 B. Bollobas, *Modern Graph Theory*, Springer-Verlag, Berlin, Germany, 1998.
24 A. Smart and J. M. Ottino, *Soft Matter*, 2008, **4**, 2125–2131.
25 D. S. Bassett, E. T. Owens, M. A. Porter, M. L. Man-ning and K. E. Daniels, *Soft Matter*, 2015, **11**, 2731.
26 Y. Huang and K. E. Daniels, *Granular Matter*, 2016, **18**, 85.
27 L. Papadopoulos, J. G. Puckett, K. E. Daniels and D. S. Bassett, *Phys. Rev. E*, 2016, **94**, 032908.
28 L. A. Pugnaloni, C. M. Carlevaro, M. Kramar, K. Mischaikow and L. Kondic, *Phys. Rev. E*, 2016, **93**, 062902.
29 L. Kondic, M. Kramar, L. A. Pugnaloni, C. M. Carlevaro and K. Mischaikow, *Phys. Rev. E*, 2016, **93**, 062903.
30 A. Tordesillas, S. T. Tobin, M. Cil, K. Alshibli and R. P. Behringer, *Phys. Rev. E*, 2015, **91**, 062204.
31 M. Herrera, S. McCarthy, S. Slotterback, E. Cephas, W. Losert and M. Girvan, *Phys. Rev. E*, 2011, **83**, 061303.
32 L. Papadopoulos, M. A. Porter, K. E. Daniels and D. S. Bassett, *Journal of Complex Networks*, 2018, cny005.
33 E. I. Corwin, H. M. Jaeger and S. R. Nagel, *Nature*, 2005, **435**, 1075.
34 D. Howell, R. P. Behringer and C. Veje, *Phys. Rev. Lett.*, 1999, **82**, 5241.
35 J. G. Puckett and K. E. Daniels, *Phys. Rev. Lett.*, 2013, **110**, 058001.
36 L. Kovalcinova, A. Goullet and L. Kondic, *Phys. Rev. E*, 2016, **93**, 042903.
37 S. Kintali, *CoRR*, 2008, abs/0809.1906.
38 *https://sites.google.com/site/bctnet/*.
39 J. G. Puckett, *Phd thesis*, North Carolina State University, 2012.
40 A. Seguin and O. Dauchot, *Phys. Rev. Lett.*, 2016, **117**, 228001.
41 *http://github.com/jekollmer/PeGS*.
42 C. Josserand, A. V. Tkachenko, D. M. Mueth and H. M. Jaeger, *Physical Review Letters*, 2000, **85**, 3632.
43 J. D. Paulsen, N. C. Keim and S. R. Nagel, *Physical Review Letters*, 2014, **113**, 068301.
44 P. Chaudhuri, L. Berthier and S. Sastry, *Physical Review Letters*, 2010, **104**, 165701.
45 T. Bertrand, R. P. Behringer, B. Chakraborty, C. S. O'Hern and M. D. Shattuck, *Physical Review E*, 2016, **93**, 012901.
46 C. Giusti, L. Papadopoulos, E. T. Owens, K. E. Daniels and D. S. Bassett, *Phys. Rev. E*, 2016, **94**, 032909.
47 V. Vitelli, N. Xu, M. Wyart, A. J. Liu and S. R. Nagel, *Phys. Rev. E*, 2010, **81**, 021301.
48 H. A. Makse, N. Gland, D. L. Johnson and L. M. Schwartz, *Phys. Rev. Lett.*, 1999, **83**, 5070–5073.
49 D. S. Bassett, E. T. Owens, K. E. Daniels and M. A. Porter, *Phys. Rev. E*, 2012, **86**, 041306.
50 O. Gendelman, Y. G. Pollack, I. Procaccia, S. Sengupta and J. Zylberg, *Phys. Rev. Lett.*, 2016, **116**, 078001.
51 E. DeGiuli and J. N. McElwaine, *Phys. Rev. Lett.*, 2016, **117**, 159801.
52 O. Gendelman, Y. G. Pollack, I. Procaccia, S. Sengupta and J. Zylberg, *Phys. Rev. Lett.*, 2016, **117**, 159802.
53 E. Falcon and B. Castaing, *American Journal of Physics*, 2005, **73**, 302–307.
54 M. E. Cates, J. P. Wittmer, J.-P. Bouchaud and P. Claudin, *Phys. Rev. Lett.*, 1998, **81**, 1841.
55 F. Zimber, J. E. Kollmer and T. Pöschel, *Phys. Rev. Lett.*, 2013, **111**, 168003.
56 D. Bi, J. Zhang, B. Chakraborty and R. P. Behringer, *Phys. Rev. Lett.*, 2013, **111**, 168003.
57 D. Bi, J. Zhang, B. Chakraborty and R. P. Behringer, *Nature*, 2011, **480**, 355–358.
58 R. Pastore, G. Pesce, A. Sasso and M. Pica Ciamarra, *The Journal of Physical Chemistry Letters*, 2017, **8**, 1562–1568.
59 M. L. Manning and A. J. Liu, *Phys. Rev. Lett.*, 2011, **107**, 108302.
60 S. Henkes, C. Brito, O. Dauchot and W. van Saarloos, *Soft Matter*, 2010, **6**, 2939–2943.